Journal of Alloys and Compounds 886 (2021) 161137

Contents lists available at ScienceDirect

Journal of Alloys and Compounds

journal homepage: www.elsevier.com/locate/jalcom

Cu_2O induced the enhancement of nonlinear absorption of MoS_2 thin film

Tingting Liu[a], Qingyou Liu[b], Ruijin Hong[a,*], Yuze Shi[a], Chunxian Tao[a], Qi Wang[a], Hui Lin[a], Zhaoxia Han[a], Dawei Zhang[a]

[a] Engineering Research Center of Optical Instrument and System, Ministry of Education and Shanghai Key Lab of Modern Optical System, University of Shanghai for Science and Technology, No. 516 Jungong Road, Shanghai 200093, China
[b] Key Laboratory of High-temperature and High-pressure Study of the Earth's Interior, Institute of Geochemistry, Chinese Academy of Sciences, Guiyang 550081, China

ARTICLE INFO

Article history:
Received 18 May 2021
Received in revised form 6 July 2021
Accepted 10 July 2021
Available online 14 July 2021

Keywords:
Cu_2O/MoS_2 composite films
Nonlinear optical response
Z-scan
Ultrafast carrier dynamics

ABSTRACT

In this paper, Cu_2O/MoS_2 composite films with excellent nonlinear properties were fabricated. X-ray diffraction, Raman scattering and scanning electron microscope results show that Cu_2O buffer layer has the effects on promoting the multiphase growth and improving both the particle size and the uniformity of MoS_2 film. The nonlinear optical response of the samples was investigated by Z-scan and ultrafast carrier dynamics, respectively. The nonlinear absorption coefficient β of Cu_2O/MoS_2 composite sample was observed to reach the maximum value of -23.08×10^{-6} cm/W, which was 24.34 and 1.76 times than that of single-layer Cu_2O and MoS_2, respectively. In addition, the nonlinear enhancement mechanism of composite samples was confirmed by the results of both transient absorption spectroscopy measurements and finite difference time domain simulation calculation.

1. Introduction

The development and application of ultrafast pulsed laser is a greatly important frontier field in modern science and technology. Especially, the emergence of femtosecond laser techniques provides a novel technical route for the exploration of the natural world. The ultrafast pulsed laser with high peak power and ultra-wide spectrum has significant applications in various fields such as industrial, scientific research, environmental, medical and extreme physical condition simulation. Saturable absorber is one of the core devices of pulsed laser, but traditional saturable absorbers such as semiconductor saturable absorber mirrors [1,2] and carbon nanotubes [3,4], are complex to prepare and have limited working bandwidth, which greatly limit their wide application. Thus, it is important to pay efforts to explore new light modulating materials with excellent saturation absorption characteristics.

As the application of graphene [5] in ultrashort pulse and mode-locked lasers continues to deepen, researchers have focused their attention on two-dimensional materials with excellent saturated absorption effects. MoS_2 is an important member of the transition metal sulfide (Transition Metal Dichalcogenides, TMDs) family. Due to its unique two-dimensional form of optical and electrical properties, as well as its availability and practicality in nature, it has become one of the most widely studied two-dimensional materials. In 2015, Zhang et al. [6] used 515 nm and 1030 nm femtosecond lasers to excite molybdenum disulfide film and found that it had a saturated absorption effect, claiming that it can be used in ultrafast photonics and fast optical switching. In recent years, nano-micron composite materials composed of metal oxides and molybdenum disulfide have a variety of excellent properties and have been applied to many fields [7–10]. As an excellent p-type semiconductor, Cu_2O (cuprous oxide) shows its excellent optical, electrical, catalytic, and sensing properties, which has attracted wide attention from researchers [11]. Therefore, many research groups prepare cuprous oxide/molybdenum disulfide nanocomposites by hydrothermal methods, focusing on the excellent absorption and charge transfer properties of the composite materials to improve their electrochemical and photocatalytic capabilities [12]. For example, Zhang et al. [13] prepared a 3D coral-like structural MoS_2/Cu_2O porous nanohybrid that showed great potential in both biosensors and electrochemical catalysts. Li et al. [14] synthesized a tunable MoS_2/Cu_2O nano-heterojunction to enhance the photochemical activity and stability of visible light. To our knowledge, there is no report

* Corresponding author.
E-mail address: rjhong@usst.edu.cn (R. Hong).

https://doi.org/10.1016/j.jallcom.2021.161137
0925-8388/

about the influence of different pulse deposition energy on the nonlinear absorption properties of Cu_2O-MoS_2 nanocomposite films.

In this study, we proposed a cost-effective route using pulsed laser ablation to modify MoS_2 sheet on the surface of the cuprous oxide film to obtain a Cu_2O/MoS_2 heterojunction. The nonlinear performance of the Cu_2O/MoS_2 composite films has been improved by changing the laser power. The influence of laser power on structure, morphology, linearity and other aspects was discussed in detail. In addition, the enhancement mechanism of the samples was analyzed through carrier dynamics and electric field distribution.

2. Experimental

2.1. Synthesis of Cu_2O-MoS_2 composite nanofilms

Prior to deposition, the K9 glass substrates were cleaned in acetone, ethanol and deionized water for 15 min in turn. Cu thin films were deposited on the substrates by electron beam evaporation from copper target (99.99%). The thickness of Cu thin film is 60 nm, and it was monitored by an in situ quartz crystal microbalance. After deposition, the as-deposited Cu film was placed in a home-made tubular furnace and annealed under ambient conditions to obtain a Cu_2O film. The annealing temperature was set at 200 °C for 2 h. The upper molybdenum disulfide was grown by laser ablation using a molybdenum disulfide target (99.9%) to obtain the Cu_2O/MoS_2 composite film. Fig. 1 shows the schematic diagram of laser ablation the above process. During laser ablation, MoS_2 target was ablated onto the surface of Cu_2O film by Nd:YAG fiber pulsed laser (YDFLP-20-M6+-S, a type of homemade laser) under ambient conditions. The wavelength of the pulsed laser is 1064 nm. The focal length, scanning rate, beam diameter and pulse width were set to 7.6, 300 mm/s, 0.1 mm and 20 ns, respectively. Moreover, the laser beam powers were set as variates with 1, 2, 3 and 4 W, respectively. These as-ablated samples were marked as Cu_2O-MoS_2-1, Cu_2O-MoS_2-2, Cu_2O-MoS_2-3 and Cu_2O-MoS_2-4, respectively. The as-annealed Cu_2O and as-ablated MoS_2 thin films were also prepared for comparison.

2.2. Characterization

The structural properties and the crystallinity of these samples are characterized by X-ray diffraction (XRD) using a Bruker AXS/D8 Advance system, with Cu Ka radiation ($\lambda = 0.15408$ nm). The UV–VIS–NIR double beam spectrophotometer (Lambda1050, PerkinElmer, USA) is used to measure the optical absorption spectrum of samples, with the scanning range of 250–1200 nm and a step length of 2 nm. In addition , the surface morphology of the samples was characterized by scanning electron microscope (SEM) (S-4800, Hitachi). Raman scattering spectra are acquired from a confocal microprobe Raman system (inVia Raman Microscope, Renishaw) with 633 nm laser excitation.

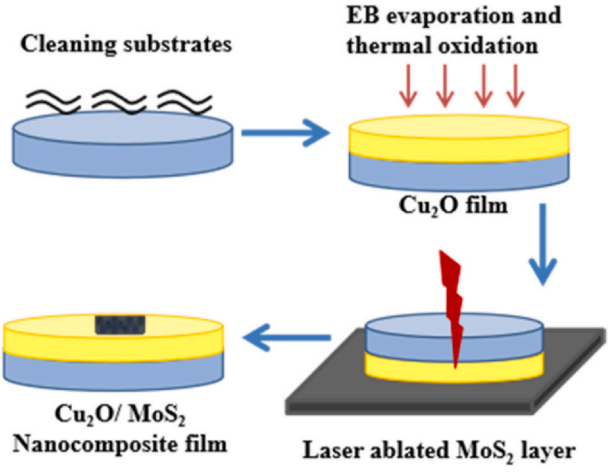

Fig. 1. The schematic diagram of preparation of Cu_2O/MoS_2 composite films.

2.3. Nonlinear optical and pump-probe measurements

The third-order nonlinear absorption coefficient is measured by a single-beam Z-scan technique based on optical distortion (self-focusing). A mode-locked picosecond laser (T-light-F9, Menlo Systems) with a wavelength of 1550 nm, a duration of 2 ps and a repetition rate of 100 MHz, was used as the optical excitation source which is focused through a 15 mm lens. What's more, a non-degenerate ultrafast optical pump-probe system was used to obtain the transient absorption spectrum of samples. In order to correlate the probe transmission with the in-band absorption of the generated electrons and holes, 400 nm and 800 nm were selected as the pump wavelength and probe wavelength, respectively, which are much lower than the exciton line. And the laser source is a 35 fs laser pulse from a mode-locked solid-state laser (SOL-35F-1K-HP-T, Spectra-Physics) with a repetition rate of 1 kHz. In the pump-probe system, both the pump and probe beams are focused onto the sample using a 75 mm focusing lens. The sample is located at the focal point of the probe beam, and the beam waist of the pump beam is 20 μm. The pump beam is chopped at 360 Hz.

3. Results and discussion

3.1. Material Characterizations

The XRD patterns as shown in Fig. 2 reveal the influence of laser ablation on the structure of Cu_2O and MoS_2. Obviously, pure cuprous oxide has only one diffraction peak at 37.4°, which corresponds to the (111) peak of the Cu_2O phase (JCPDS No. 34–1354). For as-ablated MoS_2 film, the diffraction peaks are at 15.1° and 17.0°, which can be assigned to the MoS_2(003) and Mo_2S_3(101) planes (JCPDS No.17–0972), respectively. This may be because the pulsed laser lift-off caused a small amount of S vacancies on the edge of the MoS_2 sample [15]. As for the Cu_2O/MoS_2, besides the above-mentioned peaks, more obvious peaks at about 14.5° and 41.3° are detected, corresponding to the (002) and (015) of MoS_2, respectively. It is indicated that the successful synthesis of Cu_2O/MoS_2 composite film has been confirmed, and the MoS_2 film tends to grow into multiple phases. However, the diffraction peaks of Cu_2O in composite films are visibly lower than that of the single layer Cu_2O sample, which is mainly due to the surface flaky molybdenum disulfide modified with cuprous oxide [16]. With the increase of the pulsed laser power, the intensity of the Cu_2O and MoS_2 diffraction peaks in the Cu_2O/MoS_2 composite samples increased.

In order to further illustrate the crystalline quality of the Cu_2O, MoS_2 and their composites, the Raman spectrum of all samples are also analyzed in detail, as shown in Fig. 3. As for single layer Cu_2O film, the characteristic peaks at 107, 224 and 635 cm^{-1} are associated with the non-Raman active phonon mode, lattice vibration mode and infrared allowable mode of Cu_2O [17–19], respectively. However, the Raman peak of CuO appears at 290 cm^{-1}, indicating that the surface of Cu_2O was partially oxidized. Similarly, the Raman shifts of MoS_2 at 377, 406, 453 and 178 cm^{-1} are in accordance with E^1_{2g}, A_{1g}, A_{2u} and combined vibrations of two different phonons (A_{1g}(M)–LA(M)), respectively, which indicates the existence of MoS_2 structures[15,19–21]. In the Cu_2O/MoS_2 composite films, the diffraction peaks of Cu_2O and MoS_2 are still observed. Furthermore, as shown in Fig. 3(b), the Raman peak intensity of the samples increases with the increase of the laser irradiation power, and this trend is consistent with that of the XRD pattern.

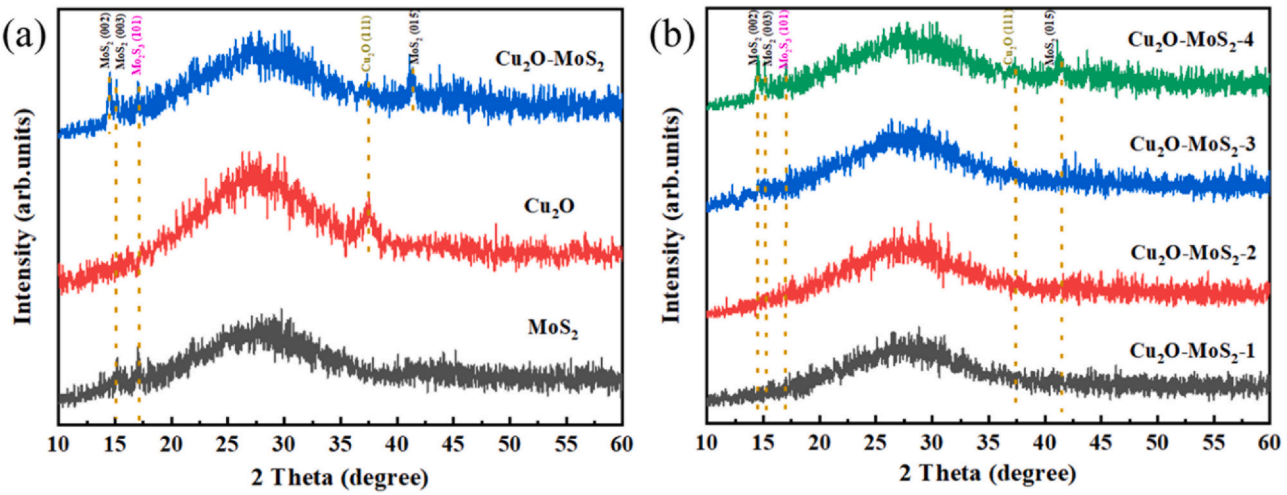

Fig. 2. The XRD patterns of (a) Cu_2O, MoS_2, Cu_2O/MoS_2 nanofilms and (b) Cu_2O/MoS_2 composite samples obtained under different laser powers.

Fig. 4 shows the SEM images of single-layer Cu_2O, MoS_2 and Cu_2O/MoS_2 composite films to characterize the surface morphology of the samples. The as-annealed Cu_2O film is relatively uniform, dense and orderly, as shown in Fig. 4(a). The deposition quality of as-ablated pure MoS_2 sample is poor, with larger particles at about 1–6 μm. It is due to the thermal effect of laser ablation that aggregates MoS_2 particles, and affects the transfer of carriers between the sample layers. For the Cu_2O/MoS_2 composite samples in Fig. 4(c-f), after laser ablation, on account of the influence of the Cu_2O base film and the inter-doping of atoms at the heterojunction interface into the lattice, the nanoparticles become smaller and are distributed in an orderly manner. The sample surface has more reactive sites and the potential barrier formed by the charge state is reduced, thereby accelerating the charge transfer between the interfaces [22,23]. With the laser power increasing, as-deposited MoS_2 particles increase, so that the particles pile up on a path wider than the scanning area. Moreover, when the power was increased to 4 W, a large number of particles gathered together, causing the surface of the sample became rough and uneven.

The corresponding absorption signals of single layer and its composite films are given in Fig. 5, reflecting the absorption of the samples in the visible light region and the performance of generating electron-hole pairs. There are two absorption peaks near 348 and 450 nm in single-layer Cu_2O film, which are caused by scattering and inter-band transitions in Cu_2O [24,25]. The as-ablated MoS_2 film has an absorption band around 366 nm corresponding to the C exciton absorption. In addition, two weak peaks could be observed at 622 nm and 676 nm from the enlarged view of MoS_2 in Fig. 5(b), representing the A (676 nm) and B (622 nm) excitons, respectively [7,21,26]. The Cu_2O-MoS_2 composite films have strong absorption in the 340–420 nm wavelength range, enhancing the absorption capacity of the entire visible light region, which is due to the synergistic effect of MoS_2 and Cu_2O[27–29]. With the laser power increasing, the absorption intensity of the Cu_2O/MoS_2 composite films increases with a red shift, as observed from Fig. 5(d).

The optical band gap of the sample is calculated by the Tauc plot between the optical band gap and the absorption spectrum. According to previous reports [4,14], Cu_2O and few-layer MoS_2 materials are direct bandgap semiconductors. It is recommended to analyze the following equation [30].

$$E_g = h\nu - \frac{(\alpha h\nu)^2}{A^2} \quad (1)$$

Here, α is absorption coefficient, h is Planck's constant, ν is the photon frequency, Eg is the optical band gap of the sample, and A is a constant. The estimated band gap energies from Tauc function of all samples are plotted in Fig. 5(c). The optical bandgaps of Cu_2O, MoS_2

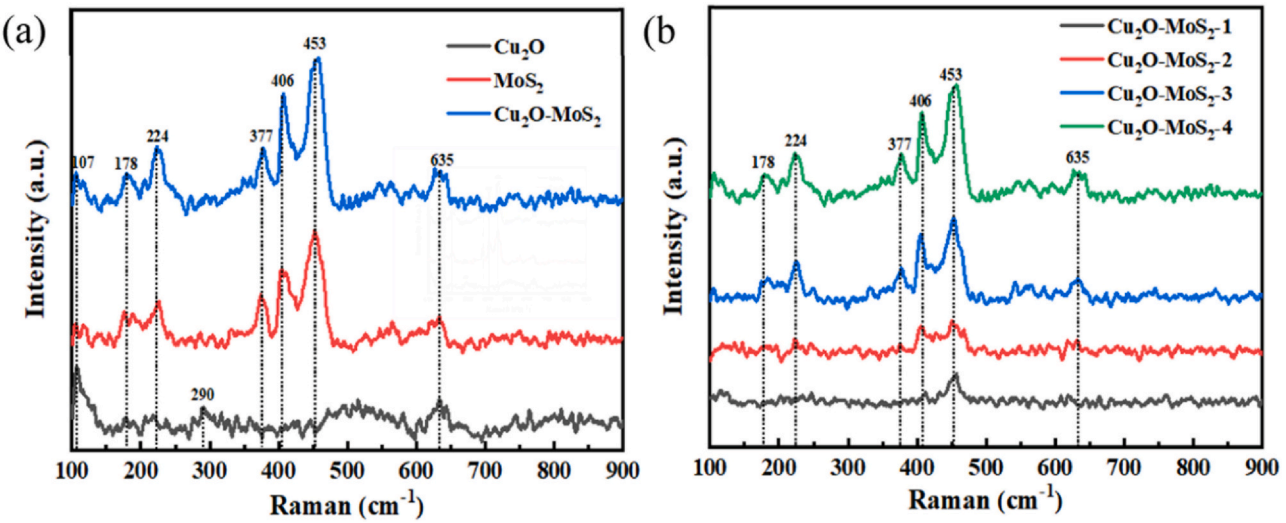

Fig. 3. Raman spectra of (a) Cu_2O, MoS_2, Cu_2O/MoS_2 nanofilms and (b) Cu_2O/MoS_2 composite samples obtained under different laser powers.

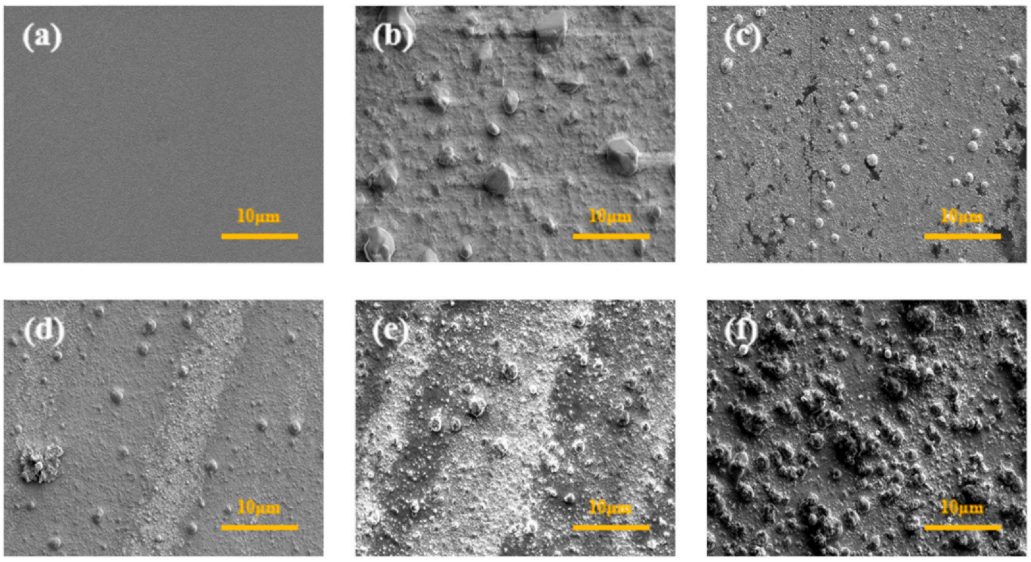

Fig. 4. The typical SEM images of (a) Cu_2O film, (b) MoS_2 film and (c-f) Cu_2O/MoS_2 composite samples obtained under different laser powers (1, 2, 3, 4 W).

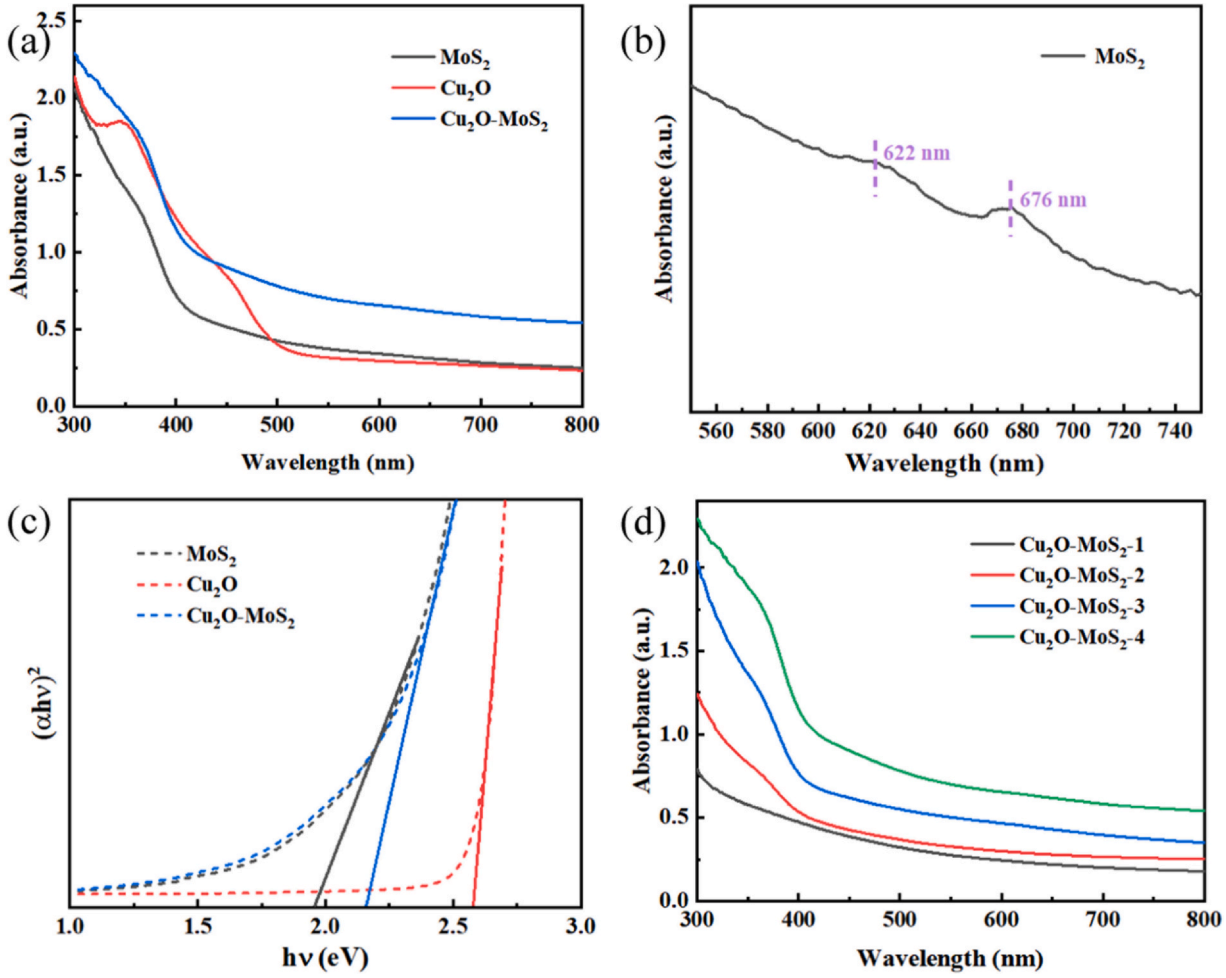

Fig. 5. The absorption spectra of (a) Cu_2O, MoS_2 and Cu_2O/MoS_2 composite films and (b) the magnified view for the 540–750 nm region of MoS_2 film. (c) Tauc plot of Cu_2O, MoS_2 and Cu_2O/MoS_2 composite films. (d) The absorption spectra of Cu_2O/MoS_2 samples with different laser powers.

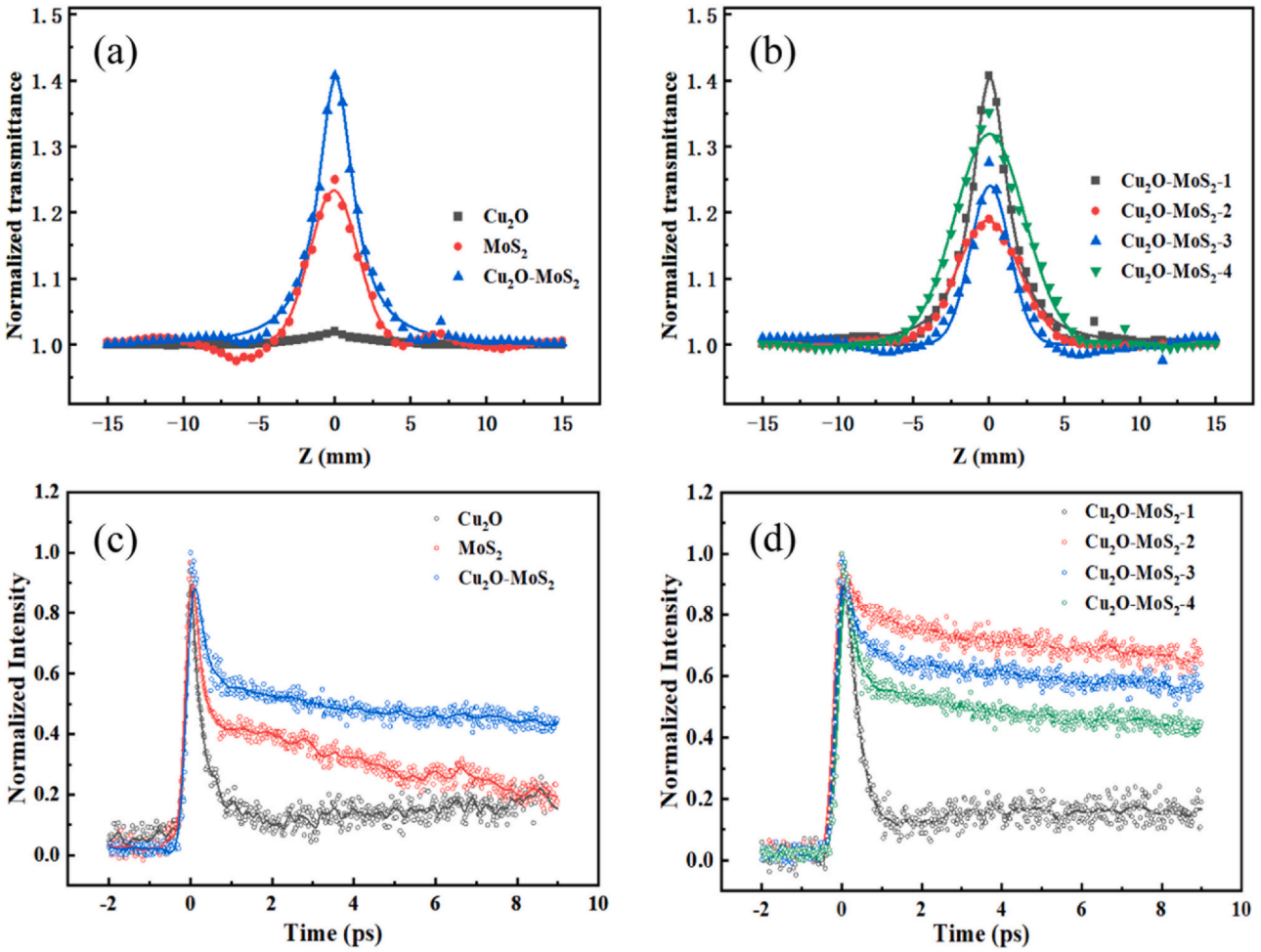

Fig. 6. (a-b) The open aperture Z-scan measurement results and (c-d) the carrier dynamics of Cu_2O, MoS_2, Cu_2O/MoS_2 composite films with different laser powers.

Table 1
The parameters obtained from the fitting of Z-scan and transient absorption results. The parameters of transient absorption are fitted using a double exponential decay function, which can be expressed as $y = A_1{}^*e^{-t/\tau 1} + A_2{}^*e^{-t/\tau 2}$.

Samples	β_{eff} (cm/W)	τ_1 (ps)	A_1	τ_2 (ps)	A_2
Cu_2O film	-9.48×10^{-7}	0.217	81%	2.47	19%
MoS_2 film	-13.06×10^{-6}	0.22	54%	10.86	46%
Cu_2O-MoS_2-1	-23.08×10^{-6}	0.32	80%	2.81	20%
Cu_2O-MoS_2-2	-9.92×10^{-6}	0.36	24%	35.11	76%
Cu_2O-MoS_2-3	-17.80×10^{-6}	0.37	35%	38.07	65%
Cu_2O-MoS_2-4	-21.69×10^{-6}	0.44	46%	40.3	54%

Table 2
The comparison of the nonlinear absorption coefficient β_{eff} values of this work with those reported in the literature.

Sample material	Wavelength (nm)	β_{eff} (cm/W)	References
Cu_2O thin film	800	4×10^{-8}	Fu et al. [33]
Cu_2O doped glasses	633	5.55×10^{-8}	Qiuling Chen [34]
MoS_2 film	800	-1.02×10^{-7}	Yang et al. [35]
Bi_2S_3/MoS_2 film	800	-1.30×10^{-7}	Yang et al. [35]
ZnO-MoS_2 film	400	11.5×10^{-7}	Liu et al. [8]
Cu_2O-MoS_2 film	1550	-23.08×10^{-6}	Current work

and Cu_2O/MoS_2 samples are estimated to be 2.58, 1.96 and 2.15 eV by a Tauc plot.

3.2. Nonlinear optical properties

In a nonlinear regime, the total nonlinear absorption coefficient of the sample can be expressed as: $\alpha = \alpha_0 + \beta I$, Where I, α_0 and β represent the incident light intensity, the linear absorption coefficient and nonlinear absorption coefficient, respectively. So the corresponding propagation equation can be represented as : $\frac{dI}{dz} = -(\alpha_0 + \beta I)I$. For the open aperture Z-scan, the normalized transmittance $T(z)$ is given by the equation:

$$T(z) = 1 - \frac{\beta I_0 L_{eff}}{2\sqrt{2}\left[1 + \left(\frac{z}{z_0}\right)^2\right]} \quad (2)$$

Here, $L_{eff} = (1 - e^{-\alpha_0 L})/\alpha_0$ is the effective optical length of the sample. Where z represents the straight-line distance between the sample and the focal point, and represents the diffraction length of the beam. Additionally, I_0 is the on-axis irradiance at the focus, and L is the thickness of the film sample.

The nonlinear absorption performance of single layer and Cu_2O/MoS_2 composite films were studied by an open aperture Z-scan system with the excitation wavelength of 1550 nm, as shown in Fig. 6(a-b). None obvious nonlinear absorption phenomenon can be observed in single layer Cu_2O sample. The MoS_2 and Cu_2O/MoS_2 composite samples showed strong saturated absorption (SA) characteristics in the open-aperture Z-scan measurement. In contrast to Cu_2O and MoS_2, the Cu_2O/MoS_2 composite films show greater transmittance under the same excitation light intensity, indicating that there is a synergistic effect between the MoS_2-Cu_2O composite films [27,31]. According to Fig. 6(b), when the laser lift-off power is smaller, the Cu_2O-MoS_2-1 sample exhibits the strongest SA effect,

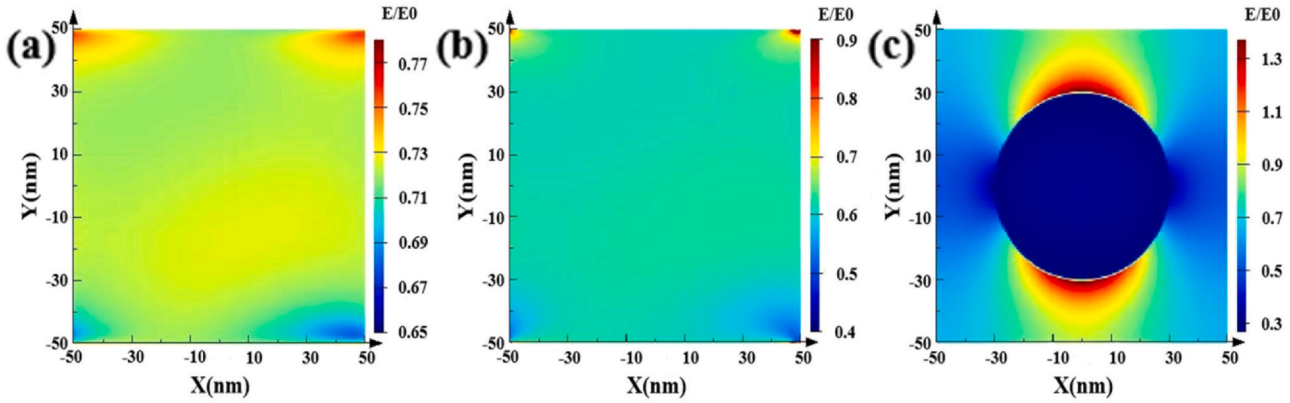

Fig. 7. FDTD simulated electric field amplitude patterns of (a) Cu_2O, (b) MoS_2 and Cu_2O/MoS_2 composite sample.

which may be due to the enhanced light-material interaction of thin layer Cu_2O/MoS_2 [32]. The nonlinear transmittance of other Cu_2O/MoS_2 samples increases with the increase of laser pulse energy.

As indicated in Table 1, compared with single-layer Cu_2O and MoS_2, the nonlinear absorption coefficient β value of Cu_2O/MoS_2 composite sample increased to -23.08×10^{-6} cm/W. It is indicated that the combination of molybdenum disulfide and cuprous oxide can effectively improve the nonlinear performance of the sample. Furthermore, we compared the current work β_{eff} value with the test values of Cu_2O and MoS_2 previously reported in the literature in Table 2. The nonlinear absorption coefficient(β) of the Cu_2O-MoS_2 film prepared in this paper is 10–100 times higher than that in previous reports [8,33–35]. It illustrates that the MoS_2 and Cu_2O-MoS_2 films prepared by pulsed laser deposition have strong saturable absorption behavior and can be used as excellent saturable absorbers.

In order to study the mechanism of the saturated absorption response of single-layer and composite samples, femtosecond transient absorption spectroscopy is used to illustrate the carrier dynamics of the samples. Fig. 6(c-d) represent the typical transient absorption spectroscopy of Cu_2O, MoS_2 and Cu_2O/MoS_2 samples. Similar to many previous reports [36–38], the carrier relaxation process of the sample can be divided into two processes: the fast relaxation time (τ_1) caused by the in-band carrier-carrier interaction and the slow relaxation (τ_2) caused by the exciton-phonon interaction. The corresponding fitting parameters are summarized in Table 1. When compared with pure Cu_2O and MoS_2 monolayers, a slower decay process is observed in the Cu_2O/MoS_2 heterojunction, and the proportion of slow relaxation time (τ_2) increases. The slow decay process in the heterostructure is attributed to the transfer of carriers from molybdenum disulfide to cuprous oxide [39], which affects the recombination of carriers in MoS_2. In addition, as the thickness of the Cu_2O/MoS_2 composite sample increases, the carrier relaxation time increases accordingly. It is attributed to the slow interlayer diffusion of excitons in the multilayer samples, which will increase the ground state bleaching effect of the sample, thereby inducing stronger saturated absorption behavior [27]. In particular, because the interlayer carrier movement accelerates when MoS_2 is thinner, the thinner Cu_2O-MoS_2-1 sample has the smallest τ_2. This trend corresponds to the Z-scan result.

Fig. 7 shows the results of finite difference time domain (FDTD) for simulate the electric field distribution of single-layer Cu_2O, MoS_2 and composite films to verify the acceleration of charge transfer in Cu_2O/MoS_2 composite samples. The surface of as-annealed Cu_2O film is dense and uniform, and the electric field intensity is only 0.73. However, the as-ablated MoS_2 sample shows the large particle size and roughness, so its local electric field strength can reach 0.9. Due to the obvious graininess and regular distribution for Cu_2O and MoS_2 composite, the local electric field intensity of Cu_2O/MoS_2 composite sample increased to 1.4. The FDTD results show that the charge transfer at the interface of Cu_2O-MoS_2 heterostructure has been significantly enhanced.

4. Conclusion

In summary, the Cu_2O/MoS_2 films were prepared by simple pulsed laser ablation. Both Raman and absorption spectra showed that the crystallinity and optical properties of the Cu_2O/MoS_2 composite samples were significantly enhanced. Open-aperture Z-scan and femtosecond transient absorption techniques were used to study the nonlinear absorption property and its carrier dynamics in Cu_2O/MoS_2 heterostructures. The electrons generated by strong light irradiation tend to transfer from molybdenum disulfide to cuprous oxide buffer layer, which can effectively accelerate the interlayer diffusion of carriers and improve the nonlinear performance of the samples.

CRediT authorship contribution statement

Tingting Liu: Writing – original draft, Software. **Qingyou Liu:** Software. **Ruijin Hong:** Writing – review & editing, Supervision. **Yuze Shi:** Data curation. **Chunxian Tao:** Formal analysis. **Qi Wang:** Formal analysis. **Hui Lin:** Formal analysis. **Zhaoxia Han:** Formal analysis. **Dawei Zhang:** Project administration, Validation.

Declaration of Competing Interest

The authors declare that they have no known competing financial interests or personal relationships that could have appeared to influence the work reported in this paper.

Acknowledgments

This work was supported by the National Natural Science Foundation of China (61775141, 62075133).

References

[1] I. Armas-Rivera, L.A. Rodriguez-Morales, M. Durán-Sánchez, M. Avazpour, A. Carrascosa, E. Silvestre, E.A. Kuzin, M.V. Andrés, B. Ibarra-Escamilla, Wide wavelength-tunable passive mode-locked Erbium-doped fiber laser with a SESAM, Opt. Laser Technol. 134 (2021) 106593, https://doi.org/10.1016/j.optlastec.2020.106593

[2] J. Wang, X. Cao, A. Xian, X. Chen, Q. Wu, Y. Liu, Z. Ge, W. Zhou, H. Wang, H. Huang, Y. Wang, W. Li, S.J. Matcher, D. Tang, D. Shen, Highly sensitive artificial visual array using transistors based on porphyrins and semiconductors, Small 17 (2021) 2005491, https://doi.org/10.1088/1612-202X/abb1bc

[3] H. Chu, Y. Li, C. Wang, H. Zhang, D. Li, Recent investigations on nonlinear absorption properties of carbon nanotubes, Nanophotonics 9 (2020) 761–781, https://doi.org/10.1515/nanoph-2020-0085

[4] V.S. Nair, A. Pusala, M. Hatamimoslehabadi, C.S. Yelleswarapu, Impact of carbon nanotube geometrical volume on nonlinear absorption and scattering properties, Opt. Mater. 73 (2017) 306–311, https://doi.org/10.1016/j.optmat.2017.08.020
[5] H. Zhang, S. Virally, Q.L. Bao, L.K. Ping, S. Massar, N. Godbout, P. Kockaert, Z-scan measurement of the nonlinear refractive index of graphene, Opt. Lett. 37 (2012) 1856–1858, https://doi.org/10.1364/ol.37.001856
[6] X. Zhang, S. Zhang, C. Chang, Y. Feng, Y. Li, N. Dong, K. Wang, L. Zhang, W.J. Blau, J. Wang, Facile fabrication of wafer-scale MoS2 neat films with enhanced third-order nonlinear optical performance, Nanoscale 7 (2015) 2978–2986, https://doi.org/10.1039/c4nr07164f
[7] X. Li, K. Hu, B. Lyu, J. Zhang, Y. Wang, P. Wang, S. Xiao, Y. Gao, J. He, Enhanced nonlinear optical response of rectangular MoS2 and MoS2/TiO2 in dispersion and film, J. Phys. Chem. C 120 (2016) 18243–18248, https://doi.org/10.1021/acs.jpcc.6b04974
[8] H.Q. Liu, C.B. Yao, G.Q. Jiang, Y. Cai, Synthesis, structure and ultrafast nonlinear absorption properties of ZnO-time/MoS2 films, J. Alloy. Compd. 847 (2020) 156524, https://doi.org/10.1016/j.jallcom.2020.156524
[9] T. Bian, J. Zhang, Z. Wang, Z. Wang, L. Liu, J. Meng, J. Zhao, Q. Cai, H. Wang, MoS2 – induced hollow Cu2O spheres: synthesis and efficient catalytic performance in the reduction of 4-nitrophenol by NaBH4, Appl. Surf. Sci. 539 (2021) 148285, https://doi.org/10.1016/j.apsusc.2020.148285
[10] S.A. Khan, T. Khan, Zulfiqar, M. Khan, Enhanced photoluminescence performance of MoS2 nanostructures after amalgamation with ZnO NPs, Optik 220 (2020) 165201, https://doi.org/10.1016/j.ijleo.2020.165201
[11] M. Mallik, S. Monia, M. Gupta, A. Ghosh, M.P. Toppo, H. Roy, Synthesis and characterization of Cu2O nanoparticles, J. Alloy. Compd. 829 (2020) 154623, https://doi.org/10.1016/j.jallcom.2020.154623
[12] L. Fang, F. Wang, Z. Chen, Y. Qiu, T. Zhai, M. Hu, C. Zhang, K. Huang, Flower-like MoS2 decorated with Cu2O nanoparticles for non-enzymatic amperometric sensing of glucose, Talanta 167 (2017) 593–599, https://doi.org/10.1016/j.talanta.2017.03.008
[13] X. Zhao, Y. Li, Y. Guo, Y. Chen, Z. Su, P. Zhang, Coral-Like MoS2/Cu2O porous nanohybrid with dual-electrocatalyst performances, Adv. Mater. Interfaces 3 (2016) 1600658, https://doi.org/10.1002/admi.201600658
[14] G. Li, W. Zhang, J. Hou, T. Li, P. Li, Y. Wang, G. Liu, K. Wang, Enhanced visible light photochemical activity and stability of MoS2/Cu2O nanocomposites by tunable heterojunction, Mater. Today Commun. 23 (2020), https://doi.org/10.1016/j.mtcomm.2020.100933
[15] B. Park, D. Lee, H.-s Kim, Y. Cho, S. Park, C. Kim, T. Lee, D.H. Woo, J.H. Kim, Synergetic enhancement in optical nonlinearity of Au nanoparticle decorated MoS2 via interaction between excitonic and surface plasmon resonances, Appl. Surf. Sci. 532 (2020) 147486, https://doi.org/10.1016/j.apsusc.2020.147486
[16] J. Luo, K. Zhang, M. Cheng, M. Gu, X. Sun, MoS2 spheres decorated on hollow porous ZnO microspheres with strong wideband microwave absorption, Chem. Eng. J. 380 (2020) 122625, https://doi.org/10.1016/j.cej.2019.122625
[17] Y. Feng, T. Jiao, J. Yin, L. Zhang, L. Zhang, J. Zhou, Q. Peng, Facile preparation of carbon nanotube-Cu2O nanocomposites as new catalyst materials for reduction of P-nitrophenol, Nanoscale Res Lett. 14 (2019) 78, https://doi.org/10.1186/s11671-019-2914-1
[18] H. Sekhar, D. Narayana Rao, Preparation, characterization and nonlinear absorption studies of cuprous oxide nanoclusters, micro-cubes and micro-particles, J. Nanopart. Res 14 (2012) 976, https://doi.org/10.1007/s11051-012-0976-4
[19] Y. Yuan, W. Wang, Y. Shi, L. Song, C. Ma, Y. Hu, The influence of highly dispersed Cu2O-anchored MoS2 hybrids on reducing smoke toxicity and fire hazards for rigid polyurethane foam, J. Hazard Mater. 382 (2020) 121028, https://doi.org/10.1016/j.jhazmat.2019.121028
[20] G. Zhang, Z. Zhang, D. Xia, Y. Qu, W. Wang, Solar driven self-sustainable photoelectrochemical bacteria inactivation in scale-up reactor utilizing large-scale fabricable Ti/MoS2/MoOx photoanode, J. Hazard Mater. 392 (2020) 122292, https://doi.org/10.1016/j.jhazmat.2020.122292
[21] C. Lu, H. Xuan, Y. Zhou, X. Xu, Q. Zhao, J. Bai, Saturable and reverse saturable absorption in molybdenum disulfide dispersion and film by defect engineering, Photonics Res. 8 (2020) 1512, https://doi.org/10.1364/prj.395870
[22] F. Li, Y. Li, J. Feng, Z. Gao, H. Lv, X. Ren, Q. Wei, Facile synthesis of MoS2@Cu2O-Pt nanohybrid as enzyme-mimetic label for the detection of the Hepatitis B surface antigen, Biosens. Bioelectron. 100 (2018) 512–518, https://doi.org/10.1016/j.bios.2017.09.048
[23] S. Zhang, H. Lu, G. Rui, C. Lv, J. He, Y. Cui, B. Gu, Preparation of Ag@ZnO core–shell nanostructures by liquid-phase laser ablation and investigation of their femtosecond nonlinear optical properties, Appl. Phys. B-Las 126 (2020), https://doi.org/10.1007/s00340-020-07490-9
[24] Y. Xiong, L. Yan, T. Chen, Nonlinear optical properties of cubic cuprous oxide with different sizes, Mater. Lett. 172 (2016) 109–111, https://doi.org/10.1016/j.matlet.2016.02.084
[25] M. Sakar, S. Balakumar, Reverse Ostwald ripening process induced dispersion of Cu2O nanoparticles in silver-matrix and their interfacial mechanism mediated sunlight driven photocatalytic properties, J. Photo Photo A 356 (2018) 150–158, https://doi.org/10.1016/j.jphotochem.2017.12.040
[26] K.P. Wang, J. Wang, J.T. Fan, M. Lotya, A. O'Neill, D. Fox, Y.Y. Feng, X.Y. Zhang, B.X. Jiang, Q.Z. Zhao, H.Z. Zhang, J.N. Coleman, L. Zhang, W.J. Blau, Ultrafast saturable absorption of two-dimensional MoS2 nanosheets, ACS Nano 7 (2013) 9260–9267, https://doi.org/10.1021/nn403886t
[27] Y. Xu, L. Yan, J. Si, M. Li, Y. Ma, J. Li, X. Hou, Nonlinear absorption properties and carrier dynamics in MoS2/Graphene van der Waals heterostructures, Carbon 165 (2020) 421–427, https://doi.org/10.1016/j.carbon.2020.04.092
[28] E.J. Yu, H.C. Kim, H.J. Kim, S.Y. Jung, K.S. Ryu, S.I. Choi, J.W. Hong, Anisotropic heteronanocrystals of Cu2O–2D MoS2 for efficient visible light driven photocatalysis, Appl. Surf. Sci. 538 (2021) 148159, https://doi.org/10.1016/j.apsusc.2020.148159
[29] M.M. He, C.J. Quan, C. He, Y.Y. Huang, L.P. Zhu, Z.H. Yao, S.J. Zhang, J.T. Bai, X.L. Xu, Enhanced nonlinear saturable absorption of MoS2/graphene nanocomposite films, J. Phys. Chem. C 121 (2017) 27147–27153, https://doi.org/10.1021/acs.jpcc.7b08850
[30] R. Szczesny, A. Scigala, B. Derkowska-Zielinska, L. Skowronski, C. Cassagne, G. Boudebs, R. Viter, E. Szlyk, Synthesis, optical, and morphological studies of ZnO powders and thin films fabricated by wet chemical methods, Materials 13 (2020), https://doi.org/10.3390/ma13112559
[31] M.E. Maldonado, A. Das, A.M. Jawaid, A.J. Ritter, R.A. Vaia, D.A. Nagaoka, P.G. Vianna, L. Seixas, C.J.S. de Matos, A. Baev, P.N. Prasad, A.S.L. Gomes, Nonlinear optical interactions and relaxation in 2D layered transition metal dichalcogenides probed by optical and photoacoustic Z-scan methods, ACS Photonics 7 (2020) 3440–3447, https://doi.org/10.1021/acsphotonics.0c01327
[32] M. Zhao, P. Song, J. Teng, Electrically and optically tunable responses in graphene/transition-metal-dichalcogenide heterostructures, ACS Appl. Mater. Inter 10 (2018) 44102–44108, https://doi.org/10.1021/acsami.8b12588
[33] M. Fu, H. Long, K. Wang, G. Yang, P. Lu, Third order optical susceptibilities of the Cu2O thin film, Thin Solid Films 519 (2011) 6557–6560, https://doi.org/10.1016/j.tsf.2011.04.209
[34] Q. Chen, Cu0&Cu2O nanoparticles functionalized diamagnetic glasses: linear/nonlinear optical, magnetic and Faraday rotation, J. Non-Cryst. Solids 543 (2020) 120156, https://doi.org/10.1016/j.jnoncrysol.2020.120156
[35] D. Yang, C. Lu, J. Ma, M. Luo, Q. Zhao, Y. Jin, X. Xu, Enhanced nonlinear saturable absorption from Type III van der Waals heterostructure Bi2S3/MoS2 by interlayer electron transition, Appl. Surf. Sci. 538 (2021) 147989, https://doi.org/10.1016/j.apsusc.2020.147989
[36] X. Dai, X. Zhang, I.M. Kislyakov, L. Wang, J. Huang, S. Zhang, N. Dong, J. Wang, Enhanced two-photon absorption and two-photon luminescence in monolayer MoS2 and WS2 by defect repairing, Opt. Express 27 (2019) 13744, https://doi.org/10.1364/oe.27.013744
[37] G. Wang, G. Liang, A.A. Baker-Murray, K. Wang, J.J. Wang, X. Zhang, D. Bennett, J.-T. Luo, J. Wang, P. Fan, W.J. Blau, Nonlinear optical performance of few-layer molybdenum diselenide as a slow-saturable absorber, Photonics Res. 6 (2018) 674, https://doi.org/10.1364/prj.6.000674
[38] X. Zhang, S. Zhang, Y. Xie, J. Huang, L. Wang, Y. Cui, J. Wang, Tailoring the nonlinear optical performance of two-dimensional MoS2 nanofilms via defect engineering, Nanoscale 10 (2018) 17924–17932, https://doi.org/10.1039/c8nr05653f
[39] J. Lin, Z. Zhang, J. Chai, B. Cao, X. Deng, W. Wang, X. Liu, G. Li, Highly efficient InGaN nanorods photoelectrode by constructing Z-scheme charge transfer system for unbiased water splitting, Small 17 (2021) 2006666, https://doi.org/10.1002/smll.202006666